



**Acoustics'08
Paris**
June 29-July 4, 2008

www.acoustics08-paris.org

Temporal approach of the synthetic aperture imaging using Hadamard matrix

Frédéric Mosca^a, Jean-Marie Nicolas^b, Laurent Kopp^c and Mathieu Couade^d

^aIxsea, 46 Quai François Mitterrand, 13600 La Ciotat, France

^bEcole Nationale Supérieure des Télécommunications de Paris, Telecom ParisTech,
Département TSI, 46 rue Barrault, 75634 Paris Cedex 13, France

^cIXwaves, 220 rue Albert Caquot, 06560 Sophia Antipolis, France

^dSupersonic Imagine, Les Jardins de la Duranne, bât E, 510, rue René Descartes, 13857
Aix-en-Provence, France

fmo@ixsea.com

The synthetic aperture imaging is a very promising solution in the well-known compromise between contrast and frame rate. Indeed this method leads to the measurement of each transmitter/receiver impulse response of the system. From this fact, synthetic aperture imaging reach the transmit/receive focus imaging quality for the cost in frame rate of the number of antenna's elements.

The main inconvenient of this method is the very low signal to noise ratio provided. Indeed, using only one transmitter per sequence leads to a very poor penetration. To correct this, a method using spatial Hadamard sequences has been introduced. For each of this Hadamard sequence, a Hadamard beam is generated in the medium.

By a temporal approach, some interesting properties of those beams are highlighted and a method using those properties is proposed. Some experiments have been done using those properties and the results show an important improvement of the frame rate for a very small cost in contrast.

1 Introduction

In classical ultrasound imaging, images are reconstructed along lines where transmitted beams are focalized at a specific depth. Image quality is optimal in a limited area given by the depth of field. Outside this area, contrast and resolution of images are significantly degraded.

A way to reduce these effects is to choose several focal lengths and partially reconstruct the image after each set of transmissions. This method, known as "multifocus imaging", improves the contrast but reduces the frame rate of the system by a factor equal to the number of selected focusing depths.

These considerations illustrate the well-known opposition between contrast and frame rate in active imaging (medical ultrasound, sonar, radar).

One very promising method used to achieve optimal homogenous image quality with a reasonable number of medium soundings is the synthetic transmit aperture (STA) [1],[2], which comprises the measurement of spatial impulse responses of the medium for every transmitter/receiver pair. In practice, one transmitter is excited at each firing, and the reflected signals are recorded on all receivers of the antenna. Each set of data is then classically delay-and-sum beamformed, providing a low resolution image for each transmit. Coherent summation of the set of low resolution images leads to the final high resolution image [3].

Another formalism, derived from a seismology approach [4], is to define a transmission matrix, with each column corresponding to the weighting vector applied at each firing. In this condition, the STA method corresponds to the identity transmission matrix. Following this track, we will call the set of data received from such a transmission the full data set (FDS) and the reception process applied in this condition, canonical beamforming.

In the first part of this article, we will compare canonical beamforming and focalized transmission/reception in terms of image quality and penetration. Then, from STA, we will derive orthogonal beamforming, which comprises sounding the medium using an invertible transmission matrix and reconstructing the image from the FDS. We will see that this method provides a noticeable improvement over canonical beamforming.

In the second part of this article, we will study the particular case of using the Hadamard matrix in

transmission. Some experimental results are provided. Finally, we will study the physics of the sounding beam in a Hadamard synthesis using a temporal approach. Some interesting properties are highlighted, and lead to a significant gain in terms of necessary number of firings, allowing to pay contrast against frame rate.

2 Orthogonal Beamforming

2.1 Focalized Transmission/Reception Case

Let's suppose that $e(\underline{x}_i, t)$ is the excitation applied to the transmitter placed at \underline{x}_i . The signal received by the receiver placed at \underline{x}_j in the case of a focal point at \underline{x} is:

$$s^f(\underline{x}_j, t) = \sum_{i=1}^N e(\underline{x}_i, t - \tau_e(\underline{x}_i, \underline{x})) \otimes h(\underline{x}_i, \underline{x}_j, t - \tau_e(\underline{x}_i, \underline{x})) + b_{th}(\underline{x}_j, t) \quad (1)$$

where N is the number of elements in the antenna and h is the impulse response of the medium integrated on the ellipse of focus $\underline{x}_i, \underline{x}_j$ and of major axis $c(t - \tau_e(\underline{x}_i, \underline{x}))$. c is the sound velocity in the medium and

$$\tau_e(\underline{x}_i, \underline{x}) = \frac{\|\underline{x} - \underline{x}_i\|}{c}.$$

If \underline{X} is a point of this ellipse and if $h(\underline{X})$ is its impulse response, then:

$$h(\underline{x}_i, \underline{x}_j, t - \tau_e(\underline{x}_i, \underline{x})) = \sum_{(\underline{X}) \in E\left(\underline{x}_i, \underline{x}_j, \frac{t - \tau_e(\underline{x}_i, \underline{x})}{c}\right)} h(\underline{X}) \quad (2)$$

Finally, b_{th} is the thermal noise generated by the sensor.

In this case, the intensity of the pixel reconstructed at the point \underline{x} , using classical delay-and-sum, is:

$$\begin{aligned} I^f(\underline{x}) &= \sum_{j=1}^N s^f(\underline{x}, \tau_r(\underline{x}, \underline{x}_j)) \\ &= \sum_{j=1}^N \sum_{i=1}^N e(\underline{x}_i, \tau_r(\underline{x}, \underline{x}_j) - \tau_e(\underline{x}_i, \underline{x})) \otimes h(\underline{x}_i, \underline{x}_j, \tau_r(\underline{x}, \underline{x}_j) - \tau_e(\underline{x}_i, \underline{x})) \\ &\quad + \sum_{j=1}^N b_{th}(\underline{x}_j, \tau_r(\underline{x}, \underline{x}_j) - \tau_e(\underline{x}_i, \underline{x})) \end{aligned} \quad (3)$$

where $\tau_r(\underline{x}, \underline{x}_j) = \frac{\|\underline{x} - \underline{x}_j\|}{c}$.

2.2 Canonical Beamforming Case

In this case, the received signal in \underline{x}_j for the i^{th} firing is:

$$s_i^c(\underline{x}_j, t) = e(\underline{x}_i, t) \otimes h(\underline{x}_i, \underline{x}_j, t) + b_{ih}^i(\underline{x}_j, t) \quad (4)$$

The pixel intensity obtained for the low resolution image is therefore:

$$I_i^C(\underline{x}) = \sum_{j=1}^N s_i^c(\underline{x}_j, \tau_r(\underline{x}, \underline{x}_j) - \tau_e(\underline{x}_i, \underline{x})) \quad (5)$$

After a coherent sum of the low-resolution images, one obtains the high resolution pixel:

$$\begin{aligned} I^C(\underline{x}) &= \sum_{i=1}^N I_i^C = \\ &= \sum_{i=1}^N \sum_{j=1}^N (e(\underline{x}_i, \tau_r(\underline{x}, \underline{x}_j) - \tau_e(\underline{x}_i, \underline{x})) \otimes h(\underline{x}_i, \underline{x}_j, \tau_r(\underline{x}, \underline{x}_j) - \tau_e(\underline{x}_i, \underline{x}))) \\ &+ \sum_{i=1}^N \sum_{j=1}^N b_{ih}^i(\underline{x}_j, \tau_r(\underline{x}, \underline{x}_j) - \tau_e(\underline{x}_i, \underline{x})) \end{aligned} \quad (6)$$

2.3 Comparison of Methods

It is easy to see that, for low-depth images, where the thermal noise can be neglected, and for a static scene, the pixel intensities are the same. Under these conditions, for the same image quality, focalized transmission / reception requires as many firings as the number of pixels, whereas canonical beamforming requires only as many firings as the number of elements in the antenna.

For the focalized transmission / reception method, the sensor noise level is:

$$B^f = \sum_{j=1}^N b_{ih}^i(\underline{x}_j, \tau_r(\underline{x}, \underline{x}_j) - \tau_e(\underline{x}_i, \underline{x})) \quad (7)$$

while for canonical beamforming, it is:

$$B^c = \sum_{i=1}^N \sum_{j=1}^N b_{ih}^i(\underline{x}_j, \tau_r(\underline{x}, \underline{x}_j) - \tau_e(\underline{x}_i, \underline{x})) \quad (8)$$

Thermal noise involves microscopic phenomena uncorrelated from one sensor to another. This noise is equidistributed on the antenna. If we assume this spatially white noise to be stationary, the standard deviations are such that:

$$\sigma_{B^c} = \sqrt{N} \sigma_{B^f} \quad (9)$$

To conclude with canonical beamforming, beyond its possible contribution to the contrast / frame rate opposition, this method presents two main disadvantages: a poor signal-to-noise ratio and a number of necessary firings that is still too large for some applications.

2.4 Orthogonal Beamforming

Let's suppose now that we use for transmitting the $N \times N$ transmission matrix $H = \{H_i\}_{i=1..N}$, with H_i being the weighting vector applied during the i^{th} firing:

$$s_i^H(\underline{x}_j, t) = \sum_{k=1}^N H(k, i) e(\underline{x}_k, t) \otimes h(\underline{x}_k, \underline{x}_j, t) + b_{ih}^i(\underline{x}_j, t) \quad (10)$$

One can see after the N acquisitions the way to build the FDS from the previous set:

$$\begin{aligned} H^{-1} * [s_1^H(\underline{x}_j, t) \dots s_N^H(\underline{x}_j, t)]^T &= K * [s_1^C(\underline{x}_j, t) \dots s_N^C(\underline{x}_j, t)]^T \\ -\sqrt{K} * [b_{ih}^1(\underline{x}_j, t) \dots b_{ih}^N(\underline{x}_j, t)]^T & \end{aligned} \quad (11)$$

where T stands for "transpose" and K is a constant called the basis gain:

$$K = \|H\| \quad (12)$$

It happens that the gain in signal-to-noise ratio is \sqrt{K} higher for orthogonal beamforming than for canonical beamforming [5].

This method provides a way to correct the poor signal-to-noise ratio of canonical beamforming but also gives us a great degree of freedom in terms of transmission pattern: orthogonal array, orthogonal non-diffracting beam family, ad hoc weighting function, Hadamard matrix....

3 Hadamard Synthesis

In the orthogonal beamforming context, one particularly interesting transmission matrix is the Hadamard matrix.

The composite transmitted signals are built from a basic pattern and its reverse (multiplied by -1). It is easy to invert (orthogonal matrix), and it provides a basis gain of N .

The Hadamard matrix is built recursively from the "seed" 2×2 matrix:

$$H_2 = \begin{pmatrix} 1 & 1 \\ 1 & -1 \end{pmatrix} \quad (13)$$

And if H_N is a $N \times N$ Hadamard matrix, then:

$$H_{2N} = \begin{pmatrix} H_N & H_N \\ H_N & -H_N \end{pmatrix} \quad (14)$$

Figure 1 shows two images acquired in the same conditions, applying canonical beamforming (left) and Hadamard beamforming (right). We can see that, at this poor penetration the image qualities are quite equivalent.

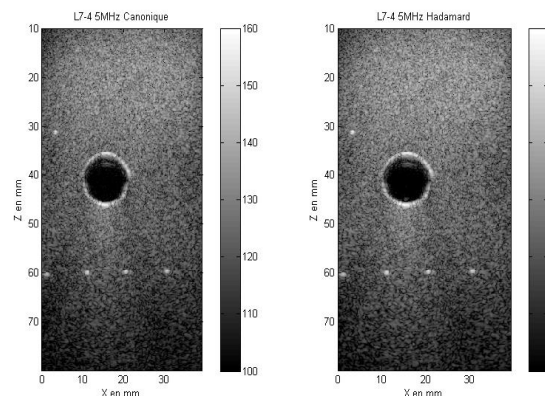


Fig.1: Comparison between canonical synthesis (left) and Hadamard synthesis (right) for a small depth.

Figure 2 shows two images acquired at a greater depth. We can see that, for sufficient depth, the canonical image reaches the thermal noise while the Hadamard image still offers a good contrast. Figure 3 shows a cut along the depth of the two images. We can see in this figure the difference of level between the two backgrounds, which is around 20dB. The probe used contains 128 elements, which confirm the basis gain approach, foreseeing a signal-to-noise ratio improvement of:

$$SNRI = 10 \cdot \log_{10}(128) = 21 \text{ dB.}$$

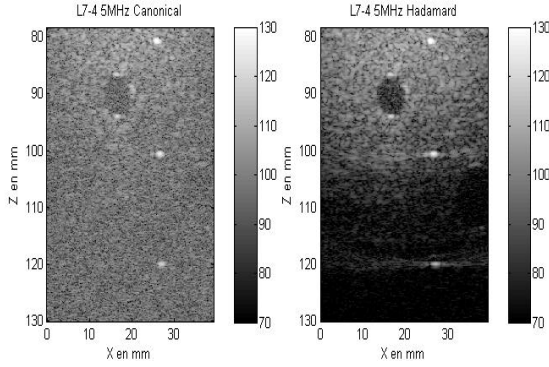


Fig.2: Canonical (left) and Hadamard synthesis (right) for a large depth.

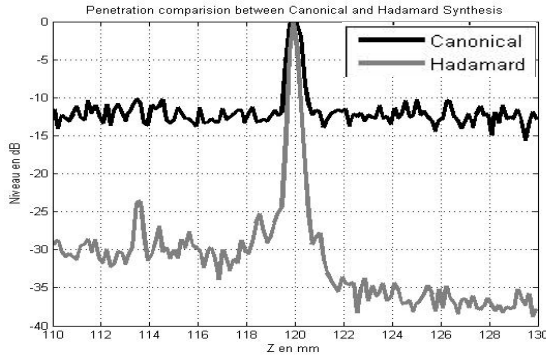


Fig.3: Cut at $x=27\text{mm}$ of Figure 3 for a large depth.

4 Temporal Approach and Properties

4.1 “Point-to-point” Huygens Principle

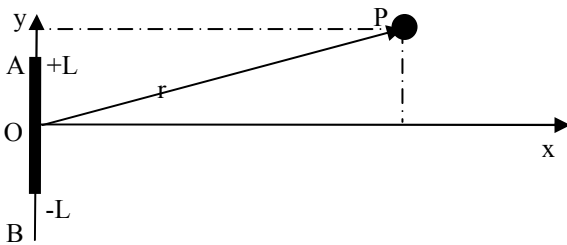


Fig.4: Linear antenna geometry.

Let's consider a radiated field from a linear antenna in far-field approximation using the geometry in Figure 4. The field amplitude at point P is given by:

$$A(x, y) = \frac{e^{jkr}}{r} \int_{-L}^L W(y_1) e^{jk \frac{yy_1}{x}} dy_1 \quad (15)$$

where W is a weighting law depending on the y_1 position and k is the wave number. If W is uniformly unitary, we can divide the antenna into two sub-antennae:

$$A(x, y) = \frac{e^{jkr}}{r} \left[\int_0^L e^{jk \frac{yy_1}{x}} dy_1 + \int_{-L}^0 e^{jk \frac{yy_1}{x}} dy_1 \right] \quad (16)$$

and by variable change:

$$A(x, y) = \frac{e^{jkr}}{r} \left[\int_0^L e^{jk \frac{yy_1}{x}} dy_1 + \int_0^L e^{jk \frac{y(y_1'-L)}{x}} dy_1' \right] \quad (17)$$

and finally:

$$A(x, y) = \frac{e^{jkr}}{r} \left(1 + e^{-jk \frac{yL}{x}} \right) \int_0^L e^{jk \frac{yy_1}{x}} dy_1 \quad (18)$$

So the zeroes of the field positions are given by the condition:

$$\frac{y}{x} = \frac{p\lambda}{2L} \quad \text{where } p \text{ is odd.} \quad (19)$$

This is a very classical result, but we can take a slightly different approach that consists in considering the fact that if the path difference between points A and O is half the wavelength, there will always be an elementary transmitter on the upper half-antenna to interfere destructively with one on the lower half antenna.

Thus zeroes of the field positions can easily be obtained considering the difference of path between the antenna extremity and the observation point.

4.2 Rank of a Hadamard Sequence

Applying a Hadamard weighting consists of dividing the total antenna in 2^{N_D} sub-antennae excited in opposition, where N_D is the Hadamard sequence rank.

With the Figure 4 geometry, a Hadamard sequence of rank N_D presents sub-antennae of size $\frac{L}{2^{N_D-1}}$.

4.3 Hadamard Sequences of Rank 1 and 2

For $N_D=1$, W is positive in the upper antenna and negative in the lower part. We can apply the “point-to-point” Huygens principle at each sub-antenna with a difference of path equal to the wavelength. The zeroes of the field positions are now situated at:

$$\frac{y}{x} = \frac{p\lambda}{2L} \quad \text{for all integers } p. \quad (20)$$

For $N_D=2$, the integral calculation gives us:

$$A(x, y) = \frac{e^{jkr}}{r} \left[\int_{\frac{L}{2}}^L e^{jk \frac{yy_1}{x}} dy_1 - \int_0^{\frac{L}{2}} e^{jk \frac{yy_1}{x}} dy_1 + \int_{\frac{L}{2}}^0 e^{jk \frac{yy_1}{x}} dy_1 - \int_{-L}^{-\frac{L}{2}} e^{jk \frac{yy_1}{x}} dy_1 \right] \quad (21)$$

By variable change:

$$A(x, y) = \frac{e^{jkr}}{r} \int_0^{\frac{L}{2}} e^{jk \frac{yy_1}{x}} dy_1 \left[e^{jk \frac{yL}{x^2}} - 1 + e^{-jk \frac{yL}{x^2}} - e^{jk \frac{yL}{x}} \right] \quad (22)$$

The conditions of zeroes are now:

$\frac{y}{x} = \frac{2p\lambda}{L}$, with p being an integer. We can note that a zero for a sequence of rank 1 is also a zero for a sequence of rank 2.

Here again, we can apply the ‘‘point-to-point’’ Huygens principle with a geometrical approach shown in Figure 5. One can easily see that the path differences are:

$$\delta_0 = \frac{L}{2} \frac{y}{x} ; \delta_1 = L \frac{y}{x} ; \delta_2 = \frac{3L}{2} \frac{y}{x}.$$

And so, destructive interference conditions are:

$$\delta_0 = p\lambda \text{ and } \delta_2 - \delta_1 = p\lambda$$

$$\text{Or: } \delta_2 - \delta_1 = \delta_0.$$

We finally find the previous condition:

$$\frac{y}{x} = \frac{2p\lambda}{L} \quad (23)$$

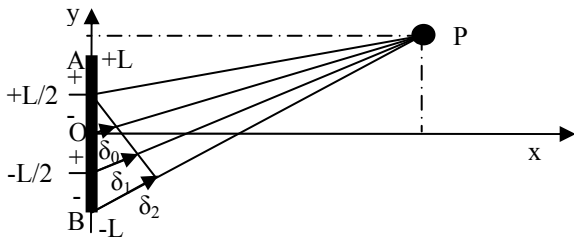


Figure 5: Rank 2 Hadamard sequence geometry.

4.4 Hadamard Sequence of Rank N

For an antenna divided in 2^N sub-antennae in two-by-two opposition, the radiated field becomes:

$$A_N(x, y) = \frac{e^{jkr}}{r} \sum_{n=-N}^{N-1} \int_{2^{n-N}L}^{2^{n+1-N}L} (-1)^n e^{jk \frac{yy_1}{x}} dy_1 \quad (24)$$

Applying the ‘‘point-to-point’’ Huygens principal in this configuration, we find the zero condition of the field in the general case:

$$\frac{y}{x} = \frac{2^{N-1} p\lambda}{L} \quad (25)$$

In other words, for a given depth, the alternance between wavefront maxima and minima is angularly doubled for each increment of the rank of the Hadamard sequence. Figure 6 represents a field radiated from an antenna of 128 elements for a Hadamard sequence of ranks 2, 3, 4, and 5.

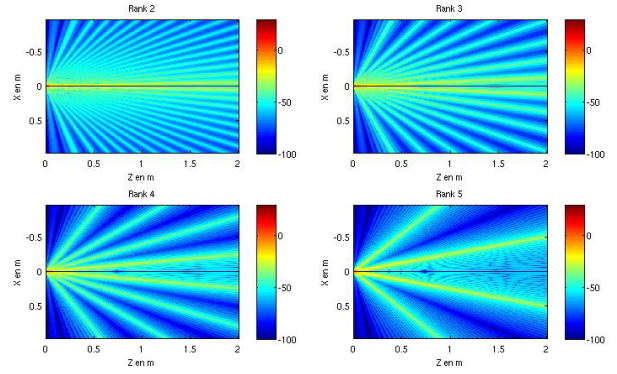


Figure 6: Radiated field for ranks 2,3, 4, and 5. Frequency is 5MHz; 128 elements; pitch is 0.3mm.

4.5 Natural Multiview

In this section, we propose to study the relationship between fields generated for rank N and $N+1$.

From (24), we have:

$$A_{N+1}(x, y) = \frac{e^{jkr}}{r} \sum_{n=-N+1}^N \int_{2^{n-N-1}L}^{2^{n-N}L} (-1)^n e^{jk \frac{yy_1}{x}} dy_1 \quad (26)$$

By variable change and development it becomes:

$$A_{N+1}(x, y) = A_N(2x, y) + (-1)^N \frac{e^{jkr}}{r} \left[2i \sin\left(2 \frac{kyL}{x}\right) \right]^{2L} \quad (27)$$

Considering the far-field approximation, we obtain the final expression:

$$A_{N+1}(x, y) = A_N(2x, y) + (-1)^N 4iky \frac{L}{x} \quad (28)$$

In other words, in the Fraunhofer area, everything happens as if the antenna was two times nearer.

Figure 7 represents cuts from Figure 6 fields at different depths. It shows evidence that the second term induces multi-scale similarity under the paraxial approximation.

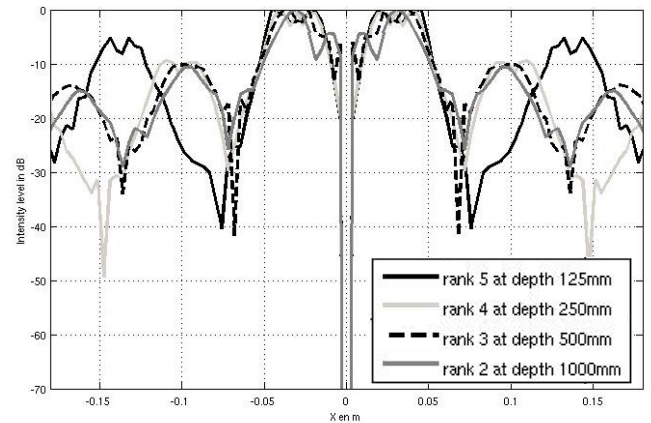


Fig.7: Transmission pattern for sequence ranks 2, 3, 4, and 5 at depths of 125, 250, 500 and 1000mm.

4.6 Fresnel Zeroes Positions

Applying the "point-to-point" Huygens method for point of interest situated along the axis of sub-antenna, it yields the following condition for the furthest Fresnel zero before the spherical decrease:

$$x = \frac{L^2 - \lambda^2}{2\lambda} \quad (29)$$

For a sequence of rank N , the position of each Fresnel zero along the axis of each sub-antenna is given by:

$$x = \frac{\frac{L^2}{2^{N-1}} - \lambda^2}{2\lambda} \quad (30)$$

Consequently, the density of energy radiated in the paraxial area will decrease very quickly for high-rank Hadamard sequences.

4.7 Lightened Hadamard Synthesis

Taking into account these previous results and benefiting from this spatial localization of the information at different sequences, one way to increase the frame rate without reducing the contrast could be to refrain from firing the high-rank Hadamard sequences.

Experimental results in Figure 8 show three images obtained by a Hadamard synthesis. The top one uses all the Hadamard sequences (128 firings), the center one uses 32 sequences, and the bottom one only uses 16 sequences.

We can see that clutter in the anechoic area is quite similar. We can see that effect of suppressing high-rank Hadamard sequence affects primarily the image in the area closest from the array.

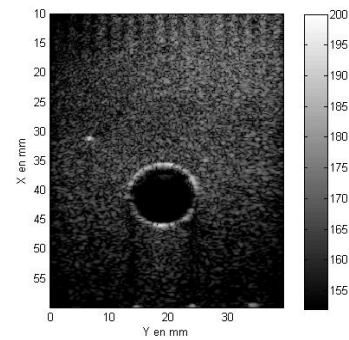
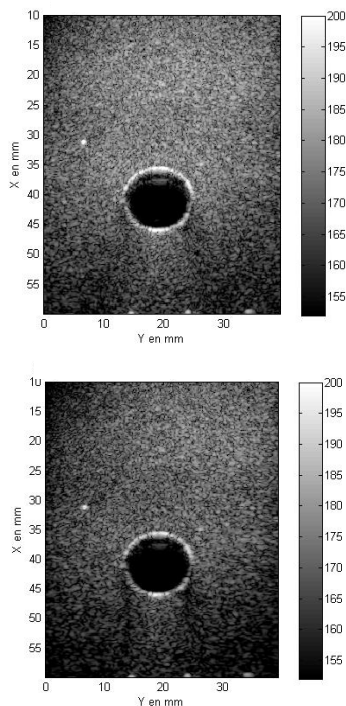


Figure 8: Upper part: Full Hadamard synthesis. Middle part: 32 sequences Hadamard synthesis Bottom part: 16 sequences Hadamard synthesis.

5 Conclusion

Coherently combining a sequence of transmissions, not necessarily reduced to a single transmit element at a time, allows us to explore new ways of imaging. This paper has dealt primarily with dynamic focusing at emission, and has shown that the Hadamard "basis" allows us to solve the energy problem and offers a methodology to keep the frame rate under control.

The transmission matrix is a promising tool to formalize "generalized" STA, aiming at new applications such as "adaptive transmission"; we foresee that it will play a part in the future for emission, similar to the "spatial filter" in reception.

The formalism will, however, have to be extended to non-scalar applications (coherent mixture) as well as to MIMO applications (non-coherent mixture).

Acknowledgements

The authors would like to thank SuperSonic Imagine, IXsea and IXwaves for their help and their support. Frédéric Mosca also wants to acknowledge the Institut TELECOM.

References

- [1] J. A. Jensen, O. Holm, L. J. Jensen, H. Bendsen, H. M. Pedersen, K. Salomonsen, J. Hansen, and S. Nikolov, "Experimental ultrasound system for real-time synthetic imaging," in *Proc IEEE Ultrason. Symp.*, 2, pp. 1595–1599, 1999
- [2] F. Gran and J. A. Jensen, "Spatial encoding using code division for fast ultrasound imaging," *IEEE Trans. Ultrason., Ferroelec., Freq. Contr* 2007
- [3] S. I. Nikolov, *Synthetic aperture tissue and flow ultrasound imaging*, Ph.D. thesis, Ørsted, DTU, 2800, Lyngby, Denmark, 2001
- [4] J. F. Claerbout, "Imaging the earth's interior," Blackwell Scientific Publications, Palo Alto, CA
- [5] R. Y. Chiao, L. J. Thomas, and S. D. Silverstein, "Sparse array imaging with spatially encoded transmits," in *Proc. IEEE Ultrason. Symp.*, 1997, pp. 1679–1682